Taylor & Francis
Taylor & Francis Group

Density-functional study of defects in two-dimensional circular nematic nanocavities

D. de las Heras[a,*], L. Mederos[b] and E. Velasco[a,c]

[a]*Departamento de Física Teórica de la Materia Condensada, Universidad Autónoma de Madrid, E-28049, Madrid, Spain;* [b]*Instituto de Ciencia de Materiales de Madrid, Consejo Superior de Investigaciones Científicas, E-28049, Madrid, Spain;* [c]*Instituto de Ciencia de Materiales Nicolás Cabrera, Universidad Autónoma de Madrid, E-28049, Madrid, Spain*

We use density-functional theory to study the structure of two-dimensional defects inside a circular nematic nanocavity. The density, nematic order parameter and director fields, as well as the defect core energy and core radius, are obtained in a thermodynamically consistent way for defects with topological charge $k = +1$ (with radial and tangential symmetries) and $k = +1/2$. An independent calculation of the fluid elastic constants, within the same theory, allows us to connect with the local free-energy density predicted by elastic theory, which in turn provides a criterion to define a defect core boundary and a defect core free energy for the two types of defects. The radial and tangential defects turn out to have very different properties, a feature that a previous Maier–Saupe theory could not account for due to the simplified nature of the interactions, which caused all elastic constants to be equal. In the case with two $k = +1/2$ defects in the cavity, the elastic regime cannot be reached due to the small radii of the cavities considered, but some trends can already be obtained.

Keywords: liquid crystals films; nanocavities; defects; elastic constants

1. Introduction

The analysis of defects in liquid crystals is very important from many points of view. In liquid-crystal applications, defects play a crucial role in governing display-cell operation. Also, there are interesting theoretical issues in different areas of physics concerning defects [1], and the stabilisation of defects has been observed and analysed in computer simulations [2–5]. A defect is a singularity in the director field of the liquid crystal [6, 7]. Local properties of the liquid crystal, e.g. the nematic order parameter, asymptotically relax to values of the bulk material far from the singularity but, in its immediate neighbourhood, properties undergo abrupt (i.e. within molecular lengths) changes; this region somehow defines microscopically a boundary for the so-called defect core.

Beyond the defect core, variations are smooth, so that the macroscopic elastic theory of Frank [8] can be used, together with some assumptions about defect core energies and radii. Very often core energies are simply ignored. It would be desirable to have estimations of these properties based on more microscopic approaches. In this context, the Landau–de Gennes [9] theory has been used extensively to predict the properties of defects, but this theory is still mesoscopic in nature and makes no contact with particle interactions. An alternative is to use computer simulations, but these are generally time consuming for the study of defects. Therefore, the formulation of theories based on molecular approaches are needed. A microscopic theory, of the Maier–Saupe type, has been advanced [10], but it has some shortcomings; for example, it predicts all

elastic constants to be equal, which causes different types of defects to have identical properties. This article is devoted to exploring the consequences of another such theory, namely a simple version of density-functional theory (DFT) for hard anisotropic particles in two dimensions, which should give more realistic values for the size and energies of defect cores since the theory predicts different values for the elastic constants.

DFT is ideally suited to the study liquid-crystal defects, since it self-consistently gives the thermodynamic and microscopic structural properties of the inhomogeneous nematic fluid. One advantage of DFT over traditional approaches is that elastic constants, in particular the problematic surface elastic constants, and other phenomenological parameters do not appear explicitly in the theory, but only implicitly through interactions and distribution functions in a free-energy functional which is minimised (to all orders in the director spatial derivatives). The defect core structure appears naturally, and this is ideal since, in contrast to the usual approximation within elastic theories of ignoring the defect cores in larger-sized nematic droplets, the contribution of defects cannot be ignored in nanocavities. One question is why details of defects should be important to understand large-scale configurations of the director field and defect motion. The microscopic approach enjoys some advantages whenever the relationship between bulk properties (such as elastic constants) and molecular structure and interaction parameters is required. Knowledge of the detailed structure of defects will not be crucial to understanding

*Corresponding author. Email: daniel.delasheras@uam.es

large-scale configurations and defect motion in stable nematics subject to boundaries or in nematic matrices where colloidal particles are embedded, but there are circumstances where this may not be so. For example, in the kinetics of defect formation, re-organisation and annihilation, it may be important to know the core structure at short length scales. The microscopic approach can give useful estimates of free-energy changes, which are necessary to study the coarsening dynamics at a more microscopic level using, for example, a relaxational dynamical equation. Also, the microscopic approach is essential at temperatures close to the clearing temperature, where defects act as nucleation seeds for the isotropic phase, and the structure and dynamics of the defects may be changing dramatically.

In DFT the structure of the fluid is summarised by the local density and orientational distribution functions, which in turn may be used to obtain the more familiar nematic order parameter and local director field; these two factors are the basic elements used to describe nematic fluids containing defects in the director field. The connection between the two descriptions is done via the local one-particle distribution function, $\rho(\mathbf{r}, \phi)$, which gives the average number of particles at some position $\mathbf{r}$ with some orientation ϕ (on the two-dimensional plane). This quantity is obtained directly from DFT, and from this all interesting fields can be extracted, for example, the microscopic director field $\widehat{\mathbf{n}}(\mathbf{r})$, which is obtained locally as the direction where the orientational part of the one-particle distribution function presents a maximum (the macroscopic nematic director could be obtained by some coarse-grained average of the latter over some appropriate volume). Therefore, the defect core region, along with the far neighbourhood of the singularity, can be analysed within a single framework based on particle interactions. The computational demands of the method are high, however, and in the present article we restrict ourselves to the case of two-dimensional cavities of small radii (in the nanometre scale).

A defect is a singularity of the nematic director field $\mathbf{n}$, characterised by a topological charge k, i.e. the number of turns of the director when the singularity is completely encircled [6]. Elastic theory assumes smooth spatial variations of the director and therefore is not able to account for the structure of the singularity. In two dimensions the local elastic free-energy density can be written as

$$f_{\text{el}}(\mathbf{r}) = \frac{1}{2}k_1(\nabla \cdot \widehat{\mathbf{n}})^2 + \frac{1}{2}k_3|\widehat{\mathbf{n}} \times (\nabla \times \widehat{\mathbf{n}})|^2, \quad (1)$$

where k_1, k_3 are elastic constants for splay and bend deformations (twist deformations are not possible in two dimensions). Let us consider the two defects with topological charge $k = +1$ depicted in Figure 1, which

are called 'radial' (r) and 'tangential' (t). If ϕ is the polar angle of the position vector $\mathbf{r}$, then the director field for the r defect is $\widehat{\mathbf{n}} = (\cos\phi, \sin\phi)$, and $\nabla \cdot \widehat{\mathbf{n}} = 1/r$, $\nabla \times \widehat{\mathbf{n}} = \mathbf{0}$, so that only splay deformations are involved. In the t defect we have $\widehat{\mathbf{n}} = (\sin\phi, -\cos\phi)$, $\nabla \cdot \widehat{\mathbf{n}} = 0$, $|\widehat{\mathbf{n}} \times (\nabla \times \widehat{\mathbf{n}})| = 1/r$, and the only deformations involved are of bend type. A general deformation will involve both modes. Now, due to the singularity at the origin (location of defect), the elastic free energy within an arbitrary area containing the origin will diverge logarithmically: elastic theory fails here, and it is necessary to subtract this region by arbitrarily defining a core region, with free energy F_n and radius r_n. The free energy within a circle or radius R will be

$$F_r = \pi k_1 \log\frac{R}{r_n^{(r)}} + F_n^{(r)},$$
$$F_t = \pi k_3 \log\frac{R}{r_n^{(t)}} + F_n^{(t)}. \quad (2)$$

For $R \to \infty$ these energies diverge logarithmically, a situation that cannot arise in practice due to the presence of defects with opposite charge in the material.

Little is known about the structure and properties of defect cores [7]. They are generally treated at a qualitative level, estimating the radius and defect core energy in an approximate way [7]. Sometimes it is assumed that these energies are negligible compared with the elastic energy, and therefore defect cores are neglected altogether, a drastic simplification which can be severe if the system size is small. One of the first attempts to describe the defect core is due to Schopohl and Sluckin [11], who analysed a 1/2-disclination using Landau–de Gennes theory with the complete ordering
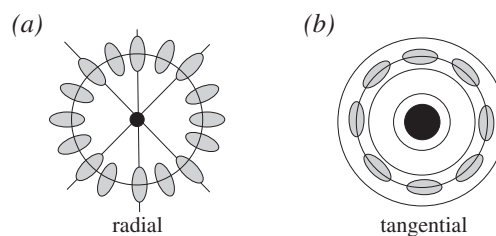

Figure 1. Schematic of the two types of defects of topological charge $k = +1$ studied in this article. (a) Radial defect, with particles pointing on average along the radial direction, which excites splay distortion mode. (b) Tangential defect, with particles pointing on average along the tangential direction, which excites the bend distortion mode. Dark circular regions represent the defect cores. Lines are tangent to the director field.

tensor $\boldsymbol{Q}$. This study demonstrated that the core of these defects does not consist of a region of isotropic material, but rather it is ordered along the disclination line (a possibility that does not exist in two dimensions). Later Monte Carlo simulations on a hard spherocylinder model by Hudson and Larson [12] corroborated this prediction, and also found a new structure with a stable triangular nucleus for very elongated molecules.

In the only truly microscopic theory presented so far, Sigillo *et al.* [10] used an approach based on a Maier–Saupe theory with an orientational distribution function, analysing disclination lines of charge $k = +1$ within a cylinder. This is a three-dimensional setup, while ours is a two-dimensional one. However, if one forgets about escape configurations, the director field should in this case exhibit the same kind of configurations as in our problem. The authors observed that the radius of the core decreases as the orientational order parameter increases. Also, they examined radial and tangential defects and analysed their cores and their energies, obtaining that the two have the same size and energy. As the authors recognise, this conclusion, which is certainly wrong, is due to the simplified interaction potential used, inherent in the Maier–Saupe theory, which predicts identical values for all the fluid elastic constants.

Despite the reduced theoretical attention received, defect cores may play a very important role in many aspects of liquid-crystal science. Mottram *et al.* [13, 14], studied disclination lines of charge $k = +1$ and $k = +1/2$ near the isotropic–nematic transition in three dimensions, and explained the impossibility of heating a nematic material above a critical temperature $T_c > T_{IN}$ (clearing point) which is below the limit of metastability of the nematic phase, owing to the growth of the isotropic core. Defect cores properties may also be relevant in dynamical aspects such as defect motion [12, 15].

In this paper we make a first attempt at calculating the properties of a defect core using a microscopic approach based on DFT, using hard-particle interactions. One of our aims is to improve upon the results of Sigillo *et al.* [10] by making more sensible predictions about the properties of the two types of defect cores investigated, namely with radial and tangential symmetries, in a circular cavity. In Section 2 we briefly review the particle model and the DFT, together with the numerical approach and the bulk behaviour. Section 3 is devoted to the calculation of the elastic constants of the model. In contrast with elastic or Landau approaches, the DFT formalism does not require the region that is the core and the region that is not the core to be specified, so that some criterion, similar to the Gibbs dividing surface in the statistical mechanics of interfaces, is needed to define the core. In

order to analyse this problem it is necessary to compare the results from DFT with elastic theory, and this demands knowledge of the splay and bend elastic constants k_1 and k_3. The values of these constants can be obtained within the same DFT framework. In Section 4 we present results for two types of point defects of charge $k = +1$ inside a circular cavity, placing emphasis on the size and energy of the defect core. Also, we discuss a configuration containing two $k = +1/2$ defects, for which no definite conclusions can be drawn (due to the cavities explored being too small) but some trends can be obtained.

2. Theory

In a previous paper [16] we have presented results for the structure, thermodynamics and structural (Frederiks) transitions of nematics confined into two-dimensional circular nanocavities using DFT. Here we use the same version of the theory in the same setup, but with an emphasis on defect core structure and energetics. Details of the theory were given in [16]; here we give a summary of the main features.

The particle model used is the hard disco-rectangle (HDR) (see Figure 2), which can be thought of as the projection of a spherocylinder on a plane. A HDR particle has a rectangular section, of length L and a diameter D, and two semicircular caps at the two ends of the rectangle, also of diameter D. These particles interact via exclusion (i.e. configurations with overlapping particles are not allowed, but particles are not interacting otherwise), and can form a two-dimensional nematic at high volume fraction [17]. As interactions are hard, the temperature dependence is trivial, so the relevant intensive variable in the thermodynamics of this fluid will be the chemical potential (or, alternatively, the density).

In DFT one writes an approximate free-energy functional $F[\rho]$ in terms of the one-particle distribution
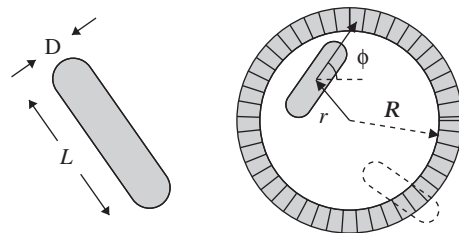

Figure 2. Schematic of a hard disco-rectangle of total length $L + D$ and width D (left), and cavity with a particle inside (right), showing the definition of the radial distance r, polar angle ϕ and cavity radius R. The dashed particle has its centre of mass right at the cavity wall and cannot move further inside the wall (i.e. inside the cavity outer region).

function $\rho(\mathbf{r}, \phi)$, which can be split as $\rho(\mathbf{r}, \phi) = \rho(\mathbf{r}) f(\mathbf{r}, \phi)$, where $f(\mathbf{r}, \phi)$ is the angular distribution function, and $\rho(\mathbf{r}) = \int d\phi \, \rho(\mathbf{r}, \phi)$ is the average local density. The free-energy functional is written as

$$F[\rho] = F_{\text{id}}[\rho] + F_{\text{exc}}[\rho] + F_{\text{ext}}[\rho] \qquad (3)$$

with $F_{\text{id}}[\rho]$ the ideal contribution,

$$\beta F_{\text{id}}[\rho] = \int_A d\mathbf{r} \, \rho(\mathbf{r}) \{ \log[\rho(\mathbf{r}) \Lambda^2 - 1] - k^{-1} S_{\text{rot}}(\mathbf{r}) \}, \qquad (4)$$

where A is the total area of the cavity, Λ the thermal wavelength and $S_{\text{rot}}(\mathbf{r})$ the local rotational entropy density:

$$S_{\text{rot}}(\mathbf{r}) = -k \int_0^{2\pi} d\phi \, f(\mathbf{r}, \phi) \log[2\pi f(\mathbf{r}, \phi)]. \qquad (5)$$

As usual, $\beta = 1/kT$, k being Boltzmann's constant. We write the excess part, $F_{\text{exc}}[\rho]$, in terms of that of a reference fluid of locally parallel hard ellipses, which in turn is obtained exactly from that of a hard-disc fluid. HDRs, ellipses and discs will be chosen to have the same particle area v and, in the case of HDRs and ellipses, the same aspect ratio. These conditions are sufficient to fix $\sigma_\parallel$ and $\sigma_\perp$, the diameters of the ellipses along the major and minor axes, respectively, and from here σ_e, the hard-disc diameter, with $\sigma_e^2 = \sigma_\parallel \sigma_\perp$. In the following we will use $\chi \equiv L/D = 15$ (which gives $L = 3.346\sigma_e$ and $D = 0.223\sigma_e$). The excess free-energy per particle of the hard-disc fluid is obtained from a theory due to Baus and Colot [18]:

$$\beta \Psi_{\text{exc}}(\eta) = (c_2 + 1)\frac{\eta}{1 - \eta} + (c_2 - 1) \log(1 - \eta), \qquad (6)$$

where $c_2 \simeq 0.1280$, $\eta = \rho_0 v$ is the packing (or volume) fraction, and ρ_0 the mean number density. The excess free energy is then written as

$$F_{\text{exc}}[\rho] = \int_A d\mathbf{r} \int_0^{2\pi} d\phi \, \rho(\mathbf{r}, \phi) \varphi(\mathbf{r}, \phi), \qquad (7)$$

where the local free-energy per particle is

$$\varphi(\mathbf{r}, \phi) = \frac{\Psi_{\text{exc}}(\eta(\mathbf{r}))}{\pi \sigma_e^2 \rho(\mathbf{r})} \int_A d\mathbf{r}' \int_0^{2\pi} d\phi' \, \rho(\mathbf{r}', \phi') \\ \times v_{\text{exc}}(\mathbf{r} - \mathbf{r}', \phi, \phi') \qquad (8)$$

Here v_{exc} is the overlap function of two HDR particles (equal to zero if particles overlap and unity otherwise).

This expression is a variation of the Parsons–Lee [19, 20] theory for homogeneous fluids of hard rods, or (from a different perspective) a variation of the Somoza–Tarazona [21] theory for inhomogeneous fluids of hard rods (both in three dimensions). Finally, $F_{\text{ext}}[\rho]$ is the contribution from the external potential (see Figure 2):

$$F_{\text{ext}}[\rho] = \int_A d\mathbf{r} \int_0^{2\pi} d\phi \, \rho(\mathbf{r}, \phi) v_{\text{ext}}(\mathbf{r}, \phi). \qquad (9)$$

The external potential acting on the particles will be chosen according to the type of favoured particle orientation at the cavity surface. In the case of the radial defect it is sufficient to use, as an external potential, a hard wall acting on the particle centres of mass:

$$v_{\text{ext}}(\mathbf{r}, \phi) = \begin{cases} \infty, & r > R, \\ 0, & r < R, \end{cases} \qquad (10)$$

where r is the radial distance measured from the centre of the cavity, and R is the radius of the circular cavity. This choice is known to favour homeotropic (i.e. perpendicular to the wall) orientation of the fluid director next to the wall [16], thus inducing an r-type defect. For the tangential defect a different choice is necessary (see Section 4.2).

The angular distribution function $f(\mathbf{r}, \phi)$ is parameterised according to

$$f(\mathbf{r}, \phi) = \frac{e^{\alpha(\mathbf{r}) \cos 2[\phi - \psi(\mathbf{r})]}}{\int_0^{2\pi} d\phi \, e^{\alpha(\mathbf{r}) \cos 2\phi}}, \qquad (11)$$

where the field $\psi(\mathbf{r})$ is the local tilt angle of the nematic director, measured with respect to the x-axis, and $\alpha(\mathbf{r})$ is a variational function, related with the local nematic order parameter $q(\mathbf{r})$ by

$$q(\mathbf{r}) = \int_0^{2\pi} d\phi \, f(\mathbf{r}, \phi) \cos\{2[\phi - \psi(\mathbf{r})]\}. \qquad (12)$$

These equations allow one to describe the configuration of the fluid by means of the three local fields $\{\rho(\mathbf{r}), q(\mathbf{r}), \psi(\mathbf{r})\}$; in the following we use the local packing fraction, $\eta(\mathbf{r}) = \pi \sigma_e^2 \rho(\mathbf{r})/4$, instead of the local density, $\rho(\mathbf{r})$, as basic density variable. Finally, for a cavity of fixed radius R, we impose on the system a constant chemical potential μ, and minimise the cavity grand potential

$$\widehat{\Omega}[\rho] = F[\rho] - \mu \int_A d\mathbf{r} \int_0^{2\pi} d\phi \, \rho(\mathbf{r}, \phi) \qquad (13)$$

with respect to variations of the variables defined above. To obtain the minimum the two-dimensional space xy is discretised into a square lattice with spacing $\Delta x = \Delta y = 0.089\sigma_e$, with mesh points (x_i, y_j), representing 40 points in a particle length $L + D$. The circular surface is approximated by a zigzag line. The trapezoidal rule was used to calculate spatial integrations, while angular integrals were approximated using Gaussian quadrature with 30–40 roots. The field variables $\{\eta(\mathbf{r}), q(\mathbf{r}), \Psi(\mathbf{r})\}$ were discretised as η_{ij}, q_{ij} and Ψ_{ij}, and the free-energy functional was minimised using the conjugate-gradient method.

This model presents a bulk isotropic–nematic phase transition for packing fraction $\eta_{IN} = 0.257$ and reduced pressure $pv_0/kT = 0.98$ (estimates from simulation [17] give $\eta_{IN} = 0.363$). The transition is of the second order.

3. Elastic constants

In order to compare with elastic theory, we need some criterion to define the boundary of the defect core. In this respect it is useful to compare the free-energy densities from DFT and elastic theory since, from this comparison, we can locate the boundary separating defect core from the outside region (where elastic theory should be valid) as the distance where both densities coincide. We see that this definition is somewhat arbitrary, as it relies on our definition of how close, numerically speaking, the two free-energy densities should be. We come to this point later. For the moment, we note that the elastic free-energy density contains elastic constants that must be known in advance. These constants have to be calculated within the same DFT scheme: the DFT free-energy density will smoothly tend to the value predicted by elastic theory provided that we use the values for elastic constants predicted by DFT. Then we calculate separately the elastic constants k_1 and k_3 in the framework of DFT. The expressions for the elastic constants are:

$$k_1 = -\frac{\Psi_{exc}(\eta_0)}{4\eta_0} \int_0^{2\pi} d\phi \int_0^{2\pi} d\phi' \rho'(\phi)\rho'(\phi') V_{yy}(\phi, \phi'),$$

$$k_3 = -\frac{\Psi_{exc}(\eta_0)}{4\eta_0} \int_0^{2\pi} d\phi \int_0^{2\pi} d\phi' \rho'(\phi)\rho'(\phi') V_{xx}(\phi, \phi'),$$

$$(14)$$

where $\eta_0 = \rho_0 v$ is the bulk packing fraction. These constants are evaluated at the uniform nematic (no spatial inhomogeneities or director distortions). The one-particle distribution function is then $\rho(\mathbf{r}, \phi) \equiv \rho(\phi) = \rho_0 f(\phi)$. In the expressions above, $\rho'(\phi)$ is the derivative of the one-particle distribution function with respect to the tilt angle, $\rho'(\phi) = \partial\rho/\partial\psi = \rho_0 \partial f/\partial\phi$, and where we defined

$$V_{ij}(\phi, \phi') \equiv \int_{\text{excluded area}} d\mathbf{r}\, v_{exc}(\mathbf{r}, \phi, \phi') x_i x_j. \quad (15)$$

The area integral over $\mathbf{r}$ is extended over the area of exclusion of two particles. Details on how these expressions are obtained can be found in Appendix A. An alternative and equivalent way to obtain the elastic constants is to use the same confinement setup (circular cavity) defined above and impose a given director field with pure splay or bend deformations (Figure 1), setting the density and nematic order parameters to the corresponding bulk values. Now if the free-energy density, as given by evaluation of the functional, is represented along any one of the cavity diameters (there is azimuthal symmetry), we can extract the elastic constants by comparing with the radial dependence predicted by elastic theory in the intermediate region (far from both the cavity centre and the cavity surface). We have seen already that the radial dependence is approximately $1/r^2$ in both cases. Since no minimisation is implicit in this method, one can use very large cavities $(R \sim 100(L + D))$ so that the elastic constants can be obtained with accuracy.

In Table 1 and Figure 3 we provide values for k_1 and k_3 (as expected, the two strategies to obtain the elastic constants explained above give the same results, except for some tiny differences that come from the numerical accuracy of angular and spatial integrals). The values of the elastic constants are zero at the bulk transition. k_3 is always larger than k_1, and their difference increases with density: when $\eta_0 \approx 0.4$ the difference is almost an order of magnitude, which means that bend deformations are more costly energetically than splay deformations. This is an important point,

Table 1. Bulk properties of nematic fluid of a HDR of aspect ratio $\chi = 15$, as obtained from DFT. Here $\Delta\mu/kT$ is the excess chemical potential with respect to the isotropic–nematic coexistence value, in units of thermal energy kT; η_0 and q are the packing fraction and nematic order parameter; and k_1/kT, k_3/kT are values of elastic constants, also in units of thermal energy.

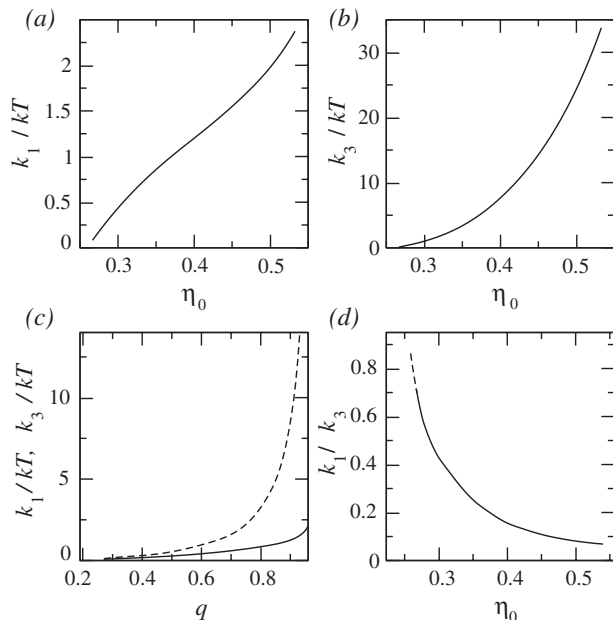| $\Delta\mu/kT$	η_0	q	k_1/kT	k_3/kT
0.15	0.270	0.27	0.08	0.11
0.75	0.303	0.63	0.47	1.13
1.75	0.360	0.83	0.93	4.05
2.75	0.410	0.90	1.27	8.72
4.25	0.470	0.94	1.70	17.8
5.25	0.503	0.96	2.01	25.2
6.25	0.533	0.97	2.38	33.8

Figure 3. Elastic constants of a nematic fluid of HDR particles with aspect ratio $\chi = 15$, as obtained from DFT. (a) Splay elastic constant k_1 in thermal energy units kT as a function of packing fraction η. (b) Bend elastic constant k_3 in thermal energy units kT as a function of packing fraction. (c) Splay (continuous line) and bend (dashed line) elastic constants as a function of nematic order parameter q. (d) Ratio of elastic constants as a function of packing fraction.

as most studies based on elastic theory assume the one-constant approximation $k_1 = k_3$. In our case (HDR particles with aspect ratio $\chi = 15$) this approximation ceases to be valid even very close to the isotropic–nematic transition (see Figure 3(d)). In confined nematics under strong geometric restrictions such as the one studied here, nematic order is very frustrated and stable nematic configurations are only obtained for conditions deep into the bulk nematic stability region (i.e. and considerably far from the bulk transition); this means that the one-constant approximation will be very inaccurate. For particles with lower aspect ratios this problem will become less acute.

One consequence of this problem can be seen in the paper by Bates [22], where the nematic ordering of hard spherocylinders lying on the surface of a sphere is examined via Monte Carlo simulation. Geometry forces the creation of four defects of charge $+1/2$. However, analysis based on the one-constant approximation predict that the defects are located at the vertices of a tetrahedron, while the simulations show that they are in fact distributed along a great circle: in this way the director field arranges itself in a way such that splay distortions are maximised, while bend distortions, much more costly energetically, are minimised.

Another observation of our calculations concerns the bulk isotropic–nematic transition. This transition has been studied by Bates and Frenkel [17] using Monte Carlo simulation. Assuming the transition to be of the Kosterlitz–Thouless type [23], and also that the two elastic constants are equal, the transition should occur when the elastic constant reaches the critical value $k_c = 8kT/\pi$. Using our values for the elastic constants and taking the average $\bar{k} = (k_1 + k_3)/2$, we obtain $\eta_{\text{IN}} = 0.36$, in perfect agreement with the simulations.

4. Results

In this section we analyse various types of defects. We start with the radial configuration, r, where only splay-type director distortions are present and there is a central defect of topological charge $k = +1$. There follows the case of charge $k = +1$ but with a tangential, t, director field. Finally, we consider point defects with charge $k = +1/2$.

4.1. *Radial defect with charge $k = +1$*

In [16] we found that this defect can only be stabilised at low chemical potential, close to the bulk isotropic–nematic transition. As the chemical potential is increased, the r configuration becomes metastable and the central $k = +1$ defect splits into two $k = +1/2$ defects. However, it is possible to impose the r configuration by preparing the system so that the director is forced to always point radially, keeping the director field unchanged during the conjugate-gradient minimisation.

An example is given in Figure 4, where the packing-fraction profile along one diameter is displayed. The different cases shown correspond to increasing cavity radius, from $R/(L + D) = 1.98$ to 7.98. Calculations are presented for fixed relative chemical potential $\Delta\mu/kT = 2.75$, where $\Delta\mu$ is referred to the value of μ at the bulk isotropic–nematic transition. Three well-defined regions can be seen. In the central region a marked depletion in number of particles is observed, which corresponds to the defect core. In the neighbourhood of this region the density is quite constant, and as the inner surface of the cavity is approached a local minimum appears, followed by a sharp density increase due to surface adsorption. Since we are mostly interested in the defect core, to minimise the effects of the surface on the core properties we need to consider as large a cavity as possible. Our present computational capabilities limit the radius of the cavity to $R \approx 10(L + D)$. However, a simple inspection of the profiles seems to indicate that the surface effects are relatively weak, even in small cavities. This figure
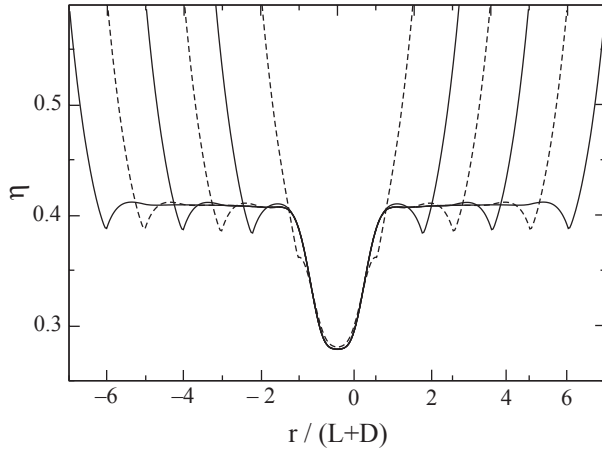
Figure 4. For a radial defect of charge $k = +1$, local packing fraction η as a function of radial distance r from the cavity centre (in units of particle length $L + D$), along an arbitrary cavity diameter, at relative chemical potential $\Delta\mu/kT = 2.75$. Lines correspond to different cavity radii: $R/(L + D) = 1.98$, 3.17, 3.98, 4.98, 5.98 and 7.98 (continuous and dashed lines alternate for a better visualisation).

Figure 5. Grand-potential density ω, in units of σ_e and kT, as a function of radial distance (in units of particle length $L + D$), along an arbitrary diameter of a cavity with $R = 7.98(L + D)$ (continuous line). The relative chemical potential is $\Delta\mu/kT = 2.75$. The dashed line is the elastic free-energy density according to elastic theory. Here r_e and r_s are approximate radial distances for the boundaries of the elastic region. The inset is a zoom of the central region.

clearly demonstrates that the size of the defect core is well defined even for cavities of small radius (say $R \gtrsim 3.2(L + D)$).

In the neighbourhood of the defect core there is a region dominated by elastic effects. If the defect were very far from any surface this region would extend up to the surface, but the question is: is it possible to obtain a truly elastic regime for small cavities such as those investigated here? To answer this question, we focus on the (grand-potential) free-energy density inside the cavity, $\omega(r)$, defined by

$$\widehat{\Omega} = \int_A d\mathbf{r}\,\omega(r). \qquad (16)$$

In Figure 5 the free-energy density is plotted as a function of radial distance from the centre of the cavity, for a cavity radius $R = 7.98(L + D)$. The elastic free-energy density $f_{el}(r) = k_1/2r^2$ is also included; to obtain this energy, the value for the k_1 elastic constant was taken from the DFT calculations (Table 1). Of course both free energies disagree in the central region of the cavity (where the free-energy density from elastic theory diverges at the singularity) and in the region close to the surface. However, there is an intermediate region, in the interval $r_e < r < r_s$ (with $r_e \simeq 2.0 - 3.0(L + D)$ and $r_s \simeq 5.0 - 5.5(L + D)$), where the agreement is quite good; this is a signature of the elastic region. The conclusion that an elastic regime can indeed be defined was also reached by Sigillo *et al.* [10] in their Maier–Saupe approach and indirectly in Landau–de Gennes
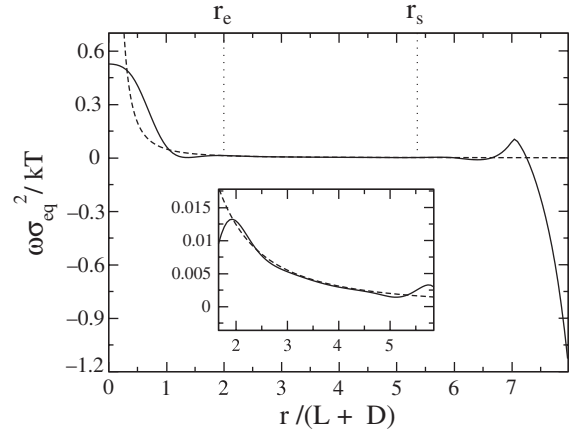
approaches [11]. The free-energy density may be used to loosely define a defect core size in terms of the radial distance at which the free-energy density begins to behave as $\sim r^{-2}$ (of course this is an ambiguous definition that, in practical terms, does not affect the numerical values of the defect core properties significantly). In the case of Figure 5 we obtain a size $2r_e \simeq 4 - 5(L + D)$; this should be a few times the correlation length ξ, which is in agreement with calculations on three-dimensional defects by Landau–de Gennes theory [11].

The properties of a cavity of radius $R = 7.98(L + D)$ are summarised in Figure 6. The profiles of the nematic order parameter, Figures 6(a) and (b), indicate that the core radius decreases as the chemical potential μ increases. To quantify this effect more precisely and analyse the depletion of the order parameter that occurs inside the central region, we have defined two additional measures of the defect core radius, $r_n^{(1)}$ and $r_n^{(2)}$, as the inflection points in the nematic order parameter and the density profiles, respectively; these two quantities do not coincide with, but should behave like, the energy-based measure r_e as thermodynamic conditions are varied). In Figure 6(c) we plot these quantities as symbols. Both have a similar behaviour: they decrease quickly with μ and saturate at high chemical potential, with the inflection point of the nematic order parameter saturating a bit earlier.

The fact that the core radius decreases with μ does not mean that its effects propagate to a smaller region; in fact, the result is quite the opposite. The difference between bulk and core densities increases with μ, while
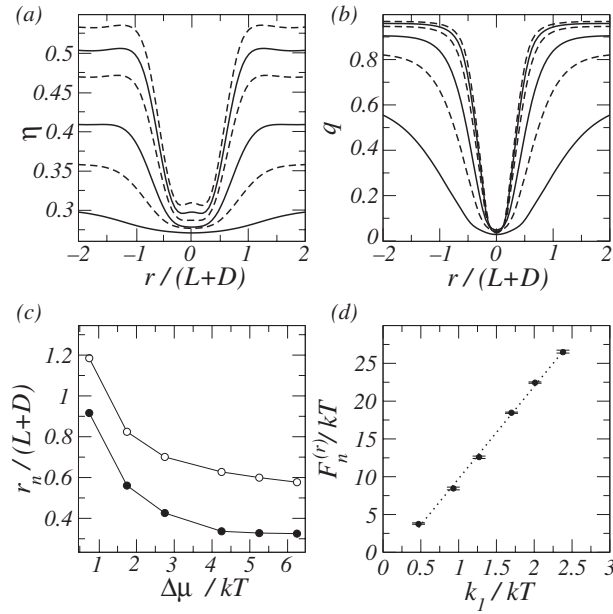
Figure 6. Some properties of a nanocavity of radius $R = 7.98(L + D)$. (a) Local packing fraction η as a function of radial distance r from the cavity centre (in units of particle length $L + D$) for various values of relative chemical potential: $\Delta\mu/kT = 0.75$, 1.75, 2.75, 4.25, 5.25 and 6.25 (from bottom to top) and for a radial defect with $k = +1$. (b) Nematic order parameter q as a function of radial distance r from the cavity centre (in units of particle length). Profiles as in panel (a). (c) Core radius r_n in units of particle length as a function of relative chemical potential. Filled circles: $r_n^{(1)}$. Open circles: $r_n^{(2)}$. (d) Core energy $F_n^{(r)}$ as function of splay elastic constant k_1, both in thermal energy units. Error bars were calculated with the two choices $r_e = 2.5(L + D)$ and $3.0(L + D)$ for the upper limit in the integral of Equation (17). The straight line is a linear fit.

the intermediate region extends to larger distances. However, the effective core radius r_e (where the free-energy density differs significantly from the elastic one) is usually in the interval $2.5 - 3(L + D)$, largely independent of μ for large $\Delta\mu$.

The successful identification of an asymptotic elastic region and the ensuing possibility of defining a defect core boundary allows us to associate a free energy F_n with the defect core. We do this by integrating the excess of grand-potential density over a uniform fluid at the same chemical potential inside a circle of radius r_e (where elastic behaviour sets in):

$$F_n = 2\pi \int_0^{r_e} dr\, r\omega(r). \tag{17}$$

This energy is represented in Figure 6(d) as a function of the elastic constant k_1. The calculation has been performed using $r = 2.75(L + D)$ as a cut-off distance, but calculations were also performed using $2.5(L + D)$ and

$3.0(L + D)$ to see the effect of changing the cut-off; error bars in the data correspond to these two limits. As can be seen in the figure, the differences are very small.

In phenomenological treatments it is usual to assume that the free energy of a disclination core of charge k is $F_n = k^2\pi\bar{k}$, where $\bar{k}$ is an elastic constant [7] in the one-constant approximation ($\bar{k} = k_1 = k_3$) which, for the radial defect, is k_1. Our DFT results give support to the linear relation between $F_n^{(r)}$ and k_1, but the slope (obtained by a linear fit) is equal to 12.2, which is four times larger than that predicted by the phenomenological theory for a point defect of charge $k = +1$. The dependence of $F_n^{(r)}$ on chemical potential is also linear, with a slope of 4.09 (not shown).

4.2.   *Tangential defect with charge $k = +1$*

In this case the director field only supports bend distortions, as shown in Figure 1. To stabilise such a structure we need a surface potential that favours planar anchoring, i.e. particle orientations tangential to the surface. We use the following model for external potential:

$$v_{\text{ext}}(r, \phi) = \begin{cases} \infty, & r > R, \\ V_0 \cos 2(\phi - \psi)e^{-\alpha(R-r)}, & r < R, \end{cases} \tag{18}$$

where V_0 is the surface strength. For large enough V_0, the surface favours tangential anchoring; we have checked that this is the case, e.g. for $V_0 = 0.7kT$ and $\alpha = 1.08(L + D)^{-1}$. These are the values we use in the following to study a defect with tangential anchoring.

The inclusion of an external field with an exponential decay means that the surface interacts with the fluid at longer distances than in the previous case. An additional feature is that, since the splay elastic constant is smaller than the bend elastic constant, the size of the defect core is larger. Both these effects play against the possibility of reaching the elastic regime in the region between the defect and the surface. Therefore, much larger cavities are needed. Our computational limit is $R \sim 15(L + D)$, which is not large enough to obtain reasonably accurate estimates of the core energy, for example. The only safe conclusion is that this energy is significantly larger than that of the radial defect.

Despite this problem, it is instructive to study the structure of the defect core in a qualitative way. Figure 7 shows the order parameter profiles in the defect core region for a cavity of radius $R = 7.98(L + D)$ (for larger cavities the profiles will be slightly different). The nematic order parameter behaves similarly as in the previous case, save the different size. The density has a pronounced maximum at the core centre. The size of the central depleted region is larger than one particle length, allowing for a higher particle concentration inside the defect core.
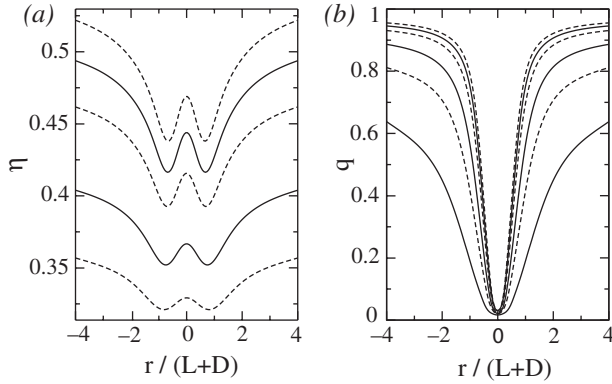
Figure 7. (a) Local packing fraction η as a function of radial distance r from the cavity centre (in units of particle length $L + D$) for various values of relative chemical potential: $\Delta\mu/kT = 0.75, 1.75, 2.75, 4.25, 5.25$ and 6.25 (from bottom to top) and for a tangential defect with $k = +1$. (b) Nematic order parameter q as a function of radial distance r from the cavity centre (in units of particle length). Profiles as in panel (a). All data pertain to the case $R = 7.98(L + D)$.

4.3. Defect with charge $k = +1/2$

The present geometry can also be used to explore a more interesting case: a defect with charge $k = +1/2$. The minimum-energy state contains two defects of charge $k = +1/2$, separated by a distance d_0, when the cavity radius is sufficiently large, but the analysis is more complicated here, as two additional minimisations are required: a partial one with respect to the 'fast' variables at fixed defect separation, and a minimisation with respect to the defect separation d_0, which is a slow variable. As a result, the computation time increases by an order of magnitude. The practical consequence is that the maximum radius of the cavity that can be analysed is reduced, and the task of splitting contributions of defect cores from the rest becomes harder.

In Figure 8 we have plotted the order parameters for a configuration with two $k = +1/2$ defects, at two different chemical potentials. The configurations were obtained by minimising the functional in a cavity of radius $R = 3.18(L + D)$ (only a region of size $30 \times 30D^2$ containing the two defect cores is shown). In the left column local packing fraction η (top), nematic order parameter (middle) and tilt angle (bottom) are shown for the case $\Delta\mu = 1.75kT$. The right column shows the same profiles when the chemical potential is increased to $\Delta\mu = 6.75kT$. In the corners of the density plots the structure has radial symmetry: this is a surface effect. This is an indication that larger cavities may be necessary for a more detailed study. We can clearly see that the core size decreases considerably as the chemical potential is increased (this effect is more visible in the nematic order parameter).
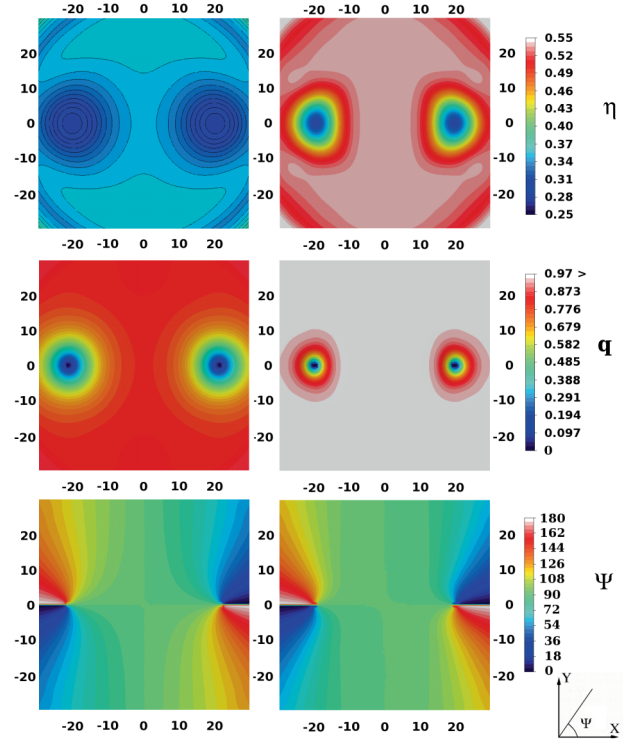

Figure 8. Contour plots with respect to xy coordinates for local packing fraction η (upper row), nematic order parameter q (middle) and director tilt angle Ψ (lower) for two configurations with relative chemical potentials $\Delta\mu = 1.75kT$ (left column) and $\Delta\mu/kT = 6.75$ (right column) in a cavity of radius $R = 3.18(L + D)$. Here xy coordinates in units of D, and the tilt angle is given in degrees.

Another remarkable effect is the loss of radial symmetry of the defect as the chemical potential is increased. The profiles in the left column (low chemical potential) have an almost radial symmetry with respect to the defect core (save the tilt angle, obviously). As μ is increased (right column), the core shrinks in all directions, especially along the direction joining the two defects, where the director field is constant.

Unfortunately, we have not yet been able to study cavities large enough for the core structure and the surface structure to relax completely to the elastic limit, but qualitative estimates can be obtained for the relevant properties of the core. This can be seen in Figure 9. In Figure 9(a) we plot the average radius of a defect core as a function of the chemical potential. Similar to the radial defect, the average radius r_n has been defined as the inflection point of the density profile, averaged over all directions (since here there is no angular symmetry). We can see that there is a rapid decay as μ increases, and r_n levels off at a value approximately equal to half the value for the radial defect (see Figure 6(c)). Therefore, the core area, which is proportional to r_n^2, is about four times less
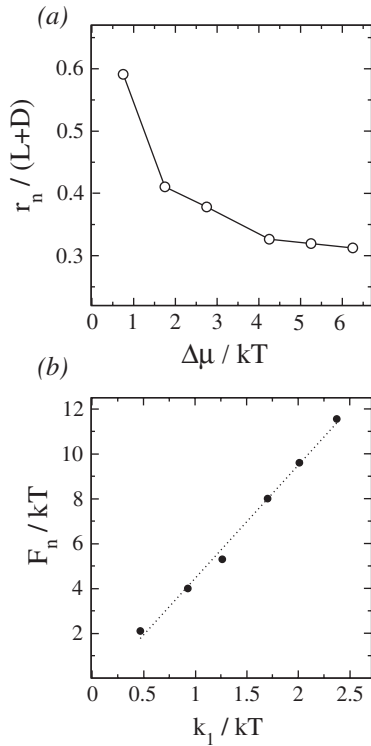
(a)

(b)

Figure 9. (a) Radius r_n as a function of relative chemical potential $\Delta\mu$, and (b) core energy F_n as a function of elastic constant k_1 for a defect of charge $k = +1/2$.

in the case $k = +1/2$ than in the case $k = 1$. In Figure 9(b) we plot the defect core energy as a function of the elastic constant k_1. The straight line is a linear regression with slope $m = 5.04$, approximately a factor 2.5 smaller than in the $k = +1$ defect. We could expect a factor of 2 beforehand, since we know in advance that, even in very small cavities, the structure with two $k = +1/2$ defects is more stable than that with a single, radial defect. In this case the largest contribution to the free energy comes from the defect cores, and therefore the energy of both cores plus their repulsive energy must be at most equal to the energy of the radial defect. We mentioned before that the defect energy is generally taken to be $F_n = k^2\pi\bar{k}$ and we would expect a factor $1/4$ in the case $k = +1/2$ with respect to the radial defect (the size is approximately four times smaller). The behaviour of the director field in the core region exhibits bend-like distortions ($\nabla \times \boldsymbol{n} \neq 0$) for $k = +1/2$, which do not appear in the radial defect and can be the origin of such a difference.

5. Summary and conclusions

In summary, we have studied the core properties of a defect in two dimensions, using a DFT (microscopic) model, free from fitting parameters, that includes consistently variations in density and nematic order parameter. All cases studied predict the formation of an isotropic region in the defect, something to be expected in two dimensions. The core free energy is proportional to the elastic constant, with a varying proportionality constant that depends on the type of defect studied; this is due to the different energetic cost associated with deformations of splay and bend type. The size of the defect cores is of the order of a few particle lengths, and decreases as the nematic ordering of the surrounding fluid increases. The core size saturates for strong nematic ordering.

The study of a two-dimensional defected nematic fluid, used here mainly for computational reasons, may be useful to understand three-dimensional phenomena in the physics of defects. As mentioned in the introduction, knowledge of the structure and energetics of defects may be important in dynamical problems, such as defect formation or nucleation and coursing of the nematic and isotropic phases. This structure may be changing in time and a microscopic approach may be helpful to follow the dynamics via relaxation equations that involve the gradient of a free energy. A natural extension of our work therefore involves the study of three-dimensional nematic fluids and their defects. Schemes where the microscopic and mesoscopic approaches are combined would also be useful in the above-mentioned problems, and work along this avenue is underway in our group.

References

[1] Trebin, H.-R. *Liq. Cryst.* **1998**, *24*, 127–130.
[2] Chiccoli, C.; Lavrentovich, O. D.; Pasini, P.; Zannoni, C. *Phys. Rev. Lett.* **1997**, *79*, 4401–4404.
[3] Billeter, J. L.; Smondyrev, A. M.; Loriot, G. B.; Pelcovits, R. A. *Phys. Rev. E* **1999**, *60*, 6831–6840.
[4] Dzubiella, J.; Schmidt, M.; Löwen, H. *Phys. Rev. E* **2000**, *62*, 5081–5091.
[5] Andrienko, D.; Allen, M. P. *Phys. Rev. E* **2002**, *61*, 504–510.
[6] Kléman, M. *Points, Lines and Walls in Liquid Crystals, Magnetic Systems and various Ordered Media*; Wiley: Chichester, 1983.
[7] Kléman, M.; Lavrentovich, O. D. *Soft Matter Physics*; Springer: New York, 2003.
[8] Frank, F. C. *Discuss. Faraday Soc.* **1958**, *25*, 19–28.
[9] de Gennes, P. G.; Prost, J. *The Physics of Liquid Crystals*; Oxford University Press: Oxford, 1995.
[10] Sigillo, I.; Greco, F.; Marrucci, G. *Liq. Cryst.* **1998**, *24*, 419–425.
[11] Schopohl, N.; Sluckin, T. J. *Phys. Rev. Lett.* **1987**, *59*, 2582–2584.

[12] Hudson, S. D.; Larson, R. G. *Phys. Rev. Lett.* **1993**, *70*, 2916–2919.

[13] Mottram, N. J.; Sluckin, T. J. *Liq. Cryst.* **2000**, *27*, 1301–1304.

[14] Mottram, N. J.; Hogan, S. J. *Phil. Trans. R. Soc. A* **1997**, *355*, 2045–2064.

[15] Tóth, G.; Denniston, C.; Yeomans, J. M. *Phys. Rev. E* **2003**, *67*, 051705–051715.

[16] de las Heras, D.; Velasco, E.; Mederos, L. *Phys. Rev. E* **2009**, *79*, 061703–061712.

[17] Bates, M. A.; Frenkel, D. *J. Chem. Phys.* **2000**, *112*, 10034–10041.

[18] Baus, M.; Colot, J.-L. *Phys. Rev. A* **1987**, *36*, 3912–3925.

[19] Parsons, J. D. *Phys. Rev. A* **1979**, *19*, 1225–1230.

[20] Lee, S. D. *J. Chem. Phys.* **1987**, *87*, 4972–4974.

[21] Somoza, A. M.; Tarazona, P. *Phys. Rev. Lett.* **1988**, *61*, 2566–2569.

[22] Bates, M. A. *J. Chem. Phys.* **2008**, *128*, 104707-1–104707-4.

[23] Stein, D. *Phys. Rev. B* **1978**, *18*, 2397–2399.

[24] Poniewierski, A.; Stecki, J. *Mol. Phys.* **1979**, *38*, 1931–1940.

[25] de las Heras, D.; Mederos, L.; Velasco, E. *Phys. Rev. E* **2003**, *68*, 031709–031718.

Appendix A. Calculation of elastic constants

Expressions for the elastic constants of a three-dimensional nematic liquid crystal were derived by Poniewierski and Stecki [24] using a direct correlation function route. From these expressions it is easy to write the corresponding two-dimensional expressions. Obtaining the direct correlation function of the theory (which, in our Onsager-type theory, is basically the Mayer function) one can obtain explicit expressions in terms of integrals over the excluded area and the orientational distribution functions. Here we present an alternative derivation, valid only in two dimensions, in terms of expansions in the local tilt angle $\psi(r)$. We start from Equations (7) and (8) for the excess free energy of a nematic with constant density, expressed explicitly in terms of the tilt angle:

$$F_{\text{exc}}[\rho] = \frac{\Psi_{\text{exc}}(\eta_0)}{4\eta_0} \int dr \int d\phi\, \rho[\phi - \psi(r)]$$
$$\times \int \int dr'\, d\phi'\, v_{\text{exc}}(r - r', \phi, \phi')\rho[\phi' - \psi(r')]. \quad (A1)$$

Now we expand the second local density $\rho(\phi' - \psi(r'))$ in $\psi(r')$ around $r' = r$. Letting $\Delta r = r' - r$, we have

$$\psi(r') = \psi(r) + \Delta r \cdot \nabla_r \psi + \frac{1}{2}[\Delta r \cdot \nabla_r]^2 \psi + \cdots. \quad (A2)$$

Then we expand the density:

$$\rho[\phi' - \psi(r')] = \rho[\phi' - \psi(r)] + \left.\frac{\partial \rho}{\partial \psi}\right|_r [\psi(r') - \psi(r)]$$
$$+ \frac{1}{2}\left.\frac{\partial^2 \rho}{\partial \psi^2}\right|_r [\psi(r') - \psi(r)]^2 + \cdots. \quad (A3)$$

Substituting (A2) and keeping terms up to third order in the gradient:

$$\rho[\phi' - \psi(r')] = \rho(\phi' - \psi(r)) + \left.\frac{\partial \rho}{\partial \psi}\right|_r$$
$$\times \left[\Delta r \cdot \nabla_r \psi + \frac{1}{2}(\Delta r \cdot \nabla_r)^2 \psi + O(\nabla_r \psi)^3 \right]$$
$$+ \frac{1}{2}\left.\frac{\partial^2 \rho}{\partial \psi^2}\right|_r$$
$$\times \left[\Delta r \cdot \nabla_r \psi + \frac{1}{2}(\Delta r \cdot \nabla_r)^2 \psi + O(\nabla_r \psi)^3 \right]^2 + \cdots$$
$$= \rho[\phi' - \psi(r)] + \rho'_\psi[\phi' - \psi(r)]\Delta r \cdot \nabla_r \psi$$
$$+ \frac{1}{2}\rho'_\psi[\phi' - \psi(r)](\Delta r \cdot \nabla_r)^2 \psi$$
$$+ \frac{1}{2}\rho''_\psi[\phi' - \psi(r)](\Delta r \cdot \nabla_r \psi)^2 + \cdots. \quad (A4)$$

The first term gives the free energy of the undistorted nematic (since $\psi(r)$ is supposed to be a slowly varying field). The elastic free energy is then

$$F_{\text{el}}[\rho] = \frac{\Psi_{\text{exc}}(\eta_0)}{8\eta_0}$$
$$\times \int \int dr\, d\phi\, \rho(\phi - \psi(r))$$
$$\times \int \int dr'\, d\phi'\, v_{\text{exc}}(r', \phi, \phi')$$
$$\times \left\{ \rho'_\psi[\phi' - \psi(r)]r' \cdot \nabla_r \psi + \frac{1}{2}\rho'_\psi[\phi' - \psi(r)][r' \cdot \nabla_r]^2 \psi \right.$$
$$\left. + \frac{1}{2}\rho''_\psi(\phi' - \psi(r))[r' \cdot \nabla_r \psi]^2 \right\}. \quad (A5)$$

We can take $\psi(r) = 0$ in the argument of the density profiles and its derivatives; the elastic free-energy density is then

$$f_{\text{d}}(r) = \frac{\Psi_{\text{exc}}(\eta_0)}{8\eta_0} \int d\phi\, \rho(\phi) \int \int dr'\, d\phi'\, v_{\text{exc}}(r', \phi, \phi')$$
$$\times \left\{ \rho'_\psi(\phi')(r' \cdot \nabla_r \psi) + \frac{1}{2}\rho'_\psi(\phi')(r' \cdot \nabla_r)^2 \psi \right.$$
$$\left. + \frac{1}{2}\rho''_\psi(\phi')(r' \cdot \nabla_r \psi)^2 \right\}. \quad (A6)$$

Now we note that

$$\int dr'\, v_{\text{exc}}(r', \phi, \phi')r' = 0, \quad (A7)$$

owing to the symmetry $V(\boldsymbol{r}, \phi, \phi') = V(-\boldsymbol{r}, \phi, \phi')$, and the term linear in the gradient of $\psi(\boldsymbol{r})$ vanishes, as it should be. Defining the dyadic

$$\widetilde{\mathcal{V}}(\phi, \phi') \equiv \int d\boldsymbol{r} \, v_{\mathrm{exc}}(\boldsymbol{r}, \phi, \phi') \boldsymbol{r}\boldsymbol{r}, \qquad (A8)$$

we obtain

$$
\begin{aligned}
F_{\mathrm{el}}[\rho] = {} & \frac{\Psi_{\mathrm{exc}}(\eta_0)}{8\eta_0} \\
& \times \sum_{\beta\gamma} \int\int d\phi \, d\phi' \mathcal{V}_{\beta\gamma}(\phi, \phi') \int d\boldsymbol{r} \, \rho(\phi - \psi(\boldsymbol{r})) \\
& \times \Big\{ \rho'_\psi[\phi' - \psi(\boldsymbol{r})] \partial_{\beta\gamma}\psi(\boldsymbol{r}) \\
& \quad + \rho''_\psi[\phi' - \psi(\boldsymbol{r})] \partial_\beta\psi(\boldsymbol{r})\partial_\gamma\psi(\boldsymbol{r}) \Big\}. \qquad (A9)
\end{aligned}
$$

Now we integrate the term with the second derivatives by parts:

$$
\begin{aligned}
& \int d\boldsymbol{r} \, \rho[\phi - \psi(\boldsymbol{r})]\rho'_\psi[\phi' - \psi(\boldsymbol{r})]\partial_{\beta\gamma}\psi(\boldsymbol{r}) \\
& = \rho[\phi - \psi(\boldsymbol{r})]\rho'_\psi[\phi' - \psi(\boldsymbol{r})]\partial_\gamma\psi(\boldsymbol{r})\Big|_{x_\beta = \mathrm{constant}} \\
& \quad - \int d\boldsymbol{r} \Big\{ \rho'_\psi[\phi - \psi(\boldsymbol{r})]\rho'_\psi[\phi' - \psi(\boldsymbol{r})] \\
& \qquad + \rho[\phi - \psi(\boldsymbol{r})]\rho''_\psi[\phi' - \psi(\boldsymbol{r})] \Big\} \partial_\beta\psi(\boldsymbol{r})\partial_\gamma\psi(\boldsymbol{r}). \\
& \qquad\qquad\qquad\qquad\qquad\qquad\qquad\qquad (A10)
\end{aligned}
$$

The $\rho\rho''$ terms in (A9) cancel out, and the surface term is neglected. Then

$$
\begin{aligned}
f_{\mathrm{el}}(\boldsymbol{r}) = {} & -\frac{\Psi_{\mathrm{exc}}(\eta_0)}{8\eta_0}\sum_{\alpha\beta\gamma\delta}\int\int d\phi \, d\phi' \, V_{\beta\gamma}(\phi, \phi') \\
& \times \rho'_\psi(\phi - \psi(\mathbf{r}))\rho'_\psi(\phi' - \psi(\mathbf{r}))\partial_\beta\psi(\mathbf{r})\partial_\gamma\psi(\mathbf{r}). \\
& \qquad\qquad\qquad\qquad\qquad\qquad\qquad\qquad (A11)
\end{aligned}
$$

which is the searched-for expression. In terms of the unit vector $\widehat{\omega}$ along the particle axis, we have $\widehat{\omega} \cdot \widehat{n} = \cos(\phi - \psi)$, and

$$
\begin{aligned}
\rho'_\psi(\phi - \psi) &= \rho'(\widehat{\omega} \cdot \widehat{\mathbf{n}})\sin(\phi - \psi), \\
\rho'_\psi(\phi' - \psi) &= \rho'(\widehat{\omega}' \cdot \widehat{\mathbf{n}})\sin(\phi' - \psi), \\
\partial_\beta(\widehat{\omega} \cdot \widehat{\mathbf{n}}) &= \sum_\alpha \omega_\alpha \partial_\beta n_\alpha = \sin(\phi - \psi)\partial_\beta\psi, \\
\partial_\gamma(\widehat{\omega}' \cdot \widehat{\mathbf{n}}) &= \sum_\delta \omega'_\delta \partial_\gamma n_\delta = \sin(\phi' - \psi)\partial_\gamma\psi,
\end{aligned}
$$

and, therefore,

$$
\begin{aligned}
\rho'_\psi(\phi - \psi)\partial_\beta\psi &= \rho'(\widehat{\omega} \cdot \widehat{\mathbf{n}})\sin(\phi - \psi)\partial_\beta\psi \\
&= \rho'(\widehat{\omega} \cdot \widehat{\mathbf{n}})\sum_\alpha \omega_\alpha\partial_\beta n_\alpha, \\
\rho'_\psi(\phi' - \psi)\partial_\gamma\psi &= \rho'(\widehat{\omega}' \cdot \widehat{\mathbf{n}})\sin(\phi' - \psi)\partial_\gamma\psi \\
&= \rho'(\widehat{\omega}' \cdot \widehat{\mathbf{n}})\sum_\delta \omega'_\delta\partial_\gamma n_\delta, \qquad (A12)
\end{aligned}
$$

so that in terms of the gradients of the nematic director:

$$
\begin{aligned}
f_{\mathrm{el}}(\boldsymbol{r}) = {} & -\frac{\Psi_{\mathrm{exc}}(\eta_0)}{8\eta_0}\sum_{\alpha\beta\gamma\delta}\int\int d\phi \, d\phi' \mathcal{V}_{\beta\gamma}(\phi, \phi') \\
& \times \rho'(\widehat{\omega} \cdot \widehat{\mathbf{n}})\rho'(\widehat{\omega}' \cdot \widehat{\mathbf{n}})\omega_\alpha\omega'_\delta\partial_\beta n_\alpha\partial_\gamma n_\delta. \\
& \qquad\qquad\qquad\qquad\qquad\qquad\qquad\qquad (A13)
\end{aligned}
$$

Since the direct correlation function of our model is

$$c(\mathbf{r}, \widehat{\omega}, \widehat{\omega}') = -\frac{\Psi_{\mathrm{exc}}(\eta_0)}{2\eta_0}v_{\mathrm{exc}}(\mathbf{r}, \widehat{\omega}, \widehat{\omega}'), \qquad (A14)$$

our expressions for k_1, k_3 coincide with the general expressions by Poniewierski and Stecki [24] using a direct correlation function route.

Now in two dimensions the Frank elastic free energy contains only splay and bend distortions:

$$f_{\mathrm{el}}(\boldsymbol{r}) = \frac{1}{2}k_1(\nabla \cdot \widehat{\boldsymbol{n}})^2 + \frac{1}{2}k_3|\nabla \times \widehat{\boldsymbol{n}}|^2. \qquad (A15)$$

Splay and bend are given, respectively, by the deformations:

$$
\begin{aligned}
(\nabla \cdot \widehat{\boldsymbol{n}})^2 &= \left(\frac{\partial n_x}{\partial x} + \frac{\partial n_y}{\partial y}\right)^2 \\
&= (\partial_x n_x)^2 + (\partial_y n_y)^2 + 2(\partial_x n_x)(\partial_y n_y), \qquad (A16)
\end{aligned}
$$

$$
\begin{aligned}
|\nabla \times \widehat{\boldsymbol{n}}|^2 &= \left(\frac{\partial n_y}{\partial x} - \frac{\partial n_x}{\partial y}\right)^2 \\
&= (\partial_x n_y)^2 + (\partial_y n_x)^2 - 2(\partial_x n_y)(\partial_y n_x),
\end{aligned}
$$

and, therefore,

$$
\begin{aligned}
k_1 &= -\frac{\Psi_{\mathrm{exc}}(\eta_0)}{4\eta_0}\int\int d\phi \, d\phi' \, \rho'(\phi)\mathcal{V}_{xx}(\phi, \phi')\rho'(\phi'), \\
k_3 &= -\frac{\Psi_{\mathrm{exc}}(\eta_0)}{4\eta_0}\int\int d\phi \, d\phi' \, \rho'(\phi)\mathcal{V}_{yy}(\phi, \phi')\rho'(\phi'). \\
& \qquad\qquad\qquad\qquad\qquad\qquad\qquad\qquad (A17)
\end{aligned}
$$

Here it is assumed that the director goes along the *x*-axis.